Supporting Figures

Supporting Figure S1: Automatic determination of CA arrival time NR_{CA} – ROI (Figure 2, 2nd step) versus pixel-based calculation. Example for the pixel-based CA arrival time, determined for each field-of-view pixel separately as outlined in the methods, mapped onto a representative tumor slice from tumor HEK #1. (**Left**) Example signal-*versus*-time-curve of a single pixel with high CNR; (**Center**) Example of the spatial localization and range of NR_{CA} values across a tumor slice, and (**Right**) corresponding NR_{CA} histogram, depicting the distribution of NR_{CA} values.

While the distribution of NR_{CA} reflects the arrival time of CA at different locations in the tumor, and thus, is reflective of plasma flow, the – compared to an average tumor slice ROI curve much noisier – signal-*versus*-time-curves may impact the robustness of this calculation significantly, as is evident from the background "NR_{CA}" outside of the tumor area. Hence, the automatic determination of CA arrival time NR_{CA} has been chosen based on the average tumor slice ROI curve, as shown in Figure 2 (2nd step).

To reduce the impact of signal disturbances at the beginning of the DCE-MRI acquisition and signal variations as a result of a significant number of pixels with a faster contrast agent arrival than the majority of pixels, potentially visible in a signal difference above noise just prior NR_{CA} (Figure 1), the first 5 and last 5 frames from NR_1 to NR_{CA} are not included in the calculation of the average pre-contrast signal, resulting in a mean pre-contrast signal (±SD) of $780.5 \cdot 10^4$ ($\pm 4.1 \cdot 10^4$) for the tumor shown here.

Supporting Figure S1

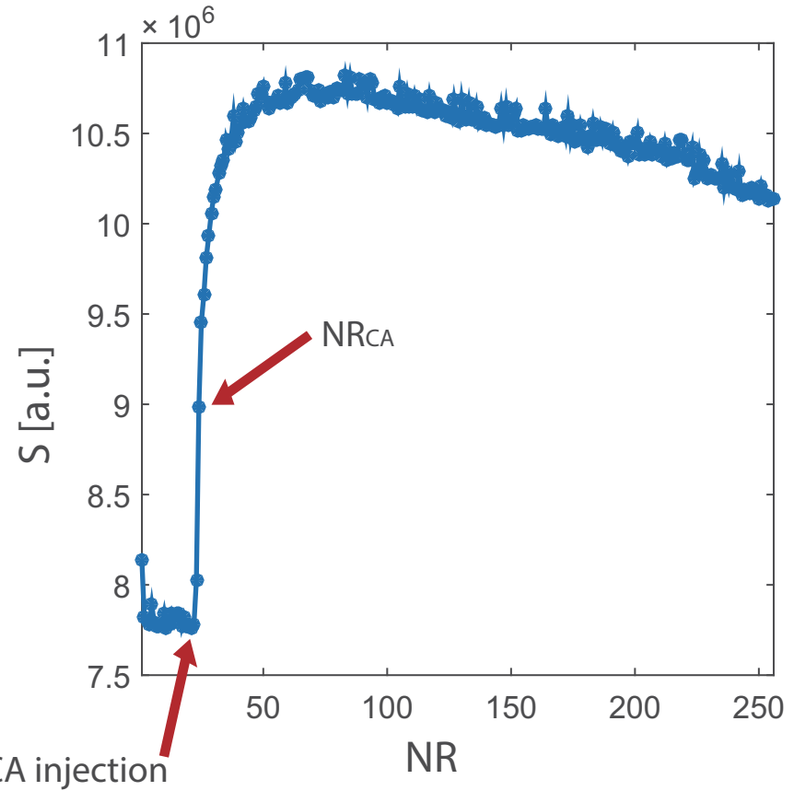

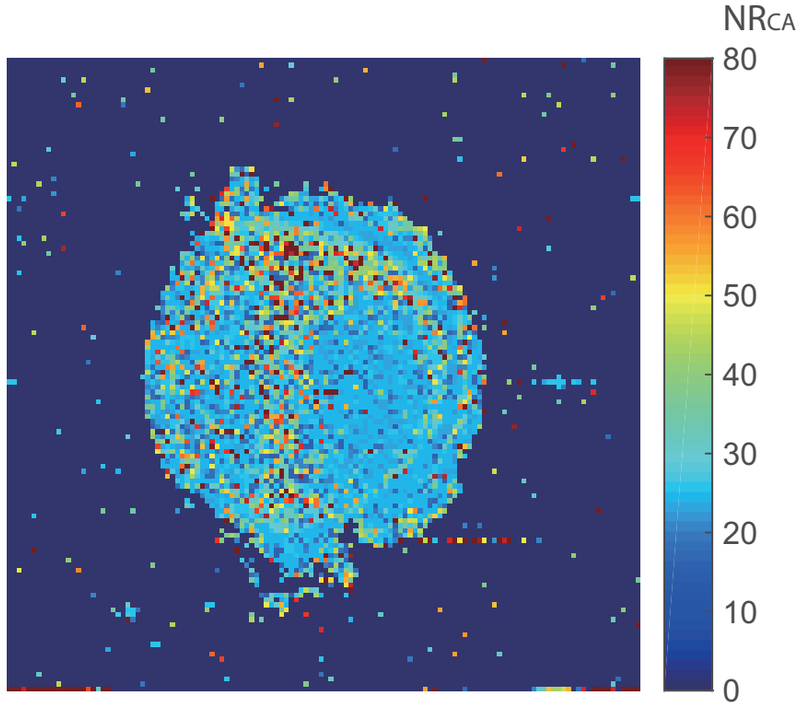

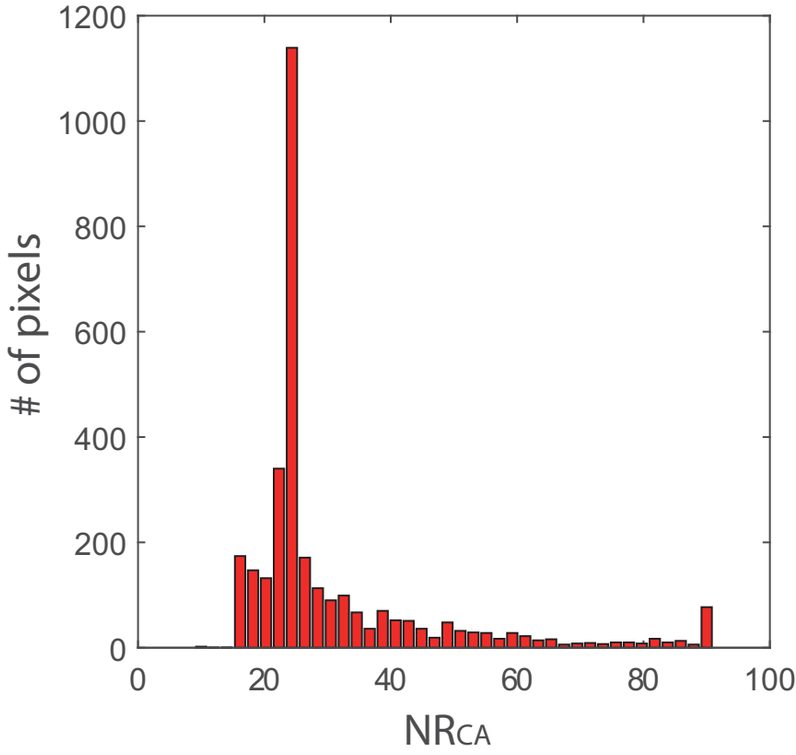

Supporting Figure S2: Validation of the automation approaches of unsupervised PR DCE-MRI analysis. Previous experimental DCE-MRI data with existing aligned *ex vivo* data (1) were reanalyzed using the new code. (**A**) Proton MR reference images of the subcutaneous hind leg tumor (1230 mm^3 by sliding-jaw caliper measurement). (**B**) The left panel shows the signal-versus-time curves for each of the three distinct patterns. On the right the corresponding weighted pattern maps are shown for each of the 5 DCE-MRI slices. (**C**) **Top row**: For the 4th slice from the left of this tumor, the three weighted pattern maps (cNMF maps 1-3) are shown enlarged with the merged pattern map shown to the right. **Bottom row:** To the *in vivo* slice shown in the top row corresponding *ex vivo* data (8 µm slice thickness) are shown. The hypoxic region shown in the 2nd panel was derived from the staining with the hypoxia marker pimonidazole (left panel). The autoradiography (3rd panel) of this tumor tissue slice depicts the accumulation of the hypoxia marker ^{18}F-Fmisonidazole, which was administered prior to tumor excision for *in vivo* hypoxia imaging using positron emission tomography (data not shown). The 4th panel shows the corresponding H&E stain, visualizing viable and necrotic tissue. The holes in the tissue correspond to the fiduciary markers used to align the *ex vivo* data with the *in vivo* data.

The automation successfully detected and mapped the three distinct CA uptake behaviors seen previously (1,2), in this case by slice-based analysis. As before a delayed wash-in/wash-out behavior of the CA (green curve in **B**) was associated with tumor hypoxia (**C**). Pixels with low to no CA uptake and no CA washout (blue curve in **B**) tend to be associated with tumor necrosis. Of note is that the merged map demonstrates the appearance of pixels with mixtures of more than one pattern, indicating that a representative 8 µm-thick *ex vivo* slice may not capture fully the intra-pixel heterogeneity in a corresponding 0.79 mm-thick *in vivo* slice.

Supporting Figure S2

A ^{1}H MRI

35 mm

B

S/S$_0$ [rel. u.]

Time [s]

C

cNMF map 1

cNMF map 2

cNMF map 3

Merged cNMF map

Pimonidazole

Hypoxic region

Autoradiography

H&E

<u>Supporting Figure S3:</u> Effect of total acquisition time on pattern recognition in DCE-MRI analysis. (**A, B**) Automatic identification of NPs, as described in Methods and Figure 2, if only the first 5 min, 10 min, or 20 min of acquisition are used respectively. Representative results with the S_{Enh} and SNR_{Th5} approaches for HEK tumor #1 are shown in (**A**). The table (**B**) lists the number of slices per total tumor slices in agreement with the manual NP determination for the six HEK tumors. The agreement between manual NP determination and NP determination by HAUC and SD_{Th} respectively was affected by shortening the total acquisition time. However, the NPs determined manually and by S_{Enh}, and SNR_{Th5} were unaffected by using only the first 5 min or 10 min of acquisition time, while agreement between manually and by SNR_{Th2} determined NPs increased using only the signal-*versus*-time-curves for the first 5 or 10 min acquisition time. (**C**) Compared to a 20 min acquisition, visualization of intra-tumoral vascular heterogeneity by PR DCE-MRI analysis using the first 5 or 10 min acquisition time demonstrates that, at a respective temporal resolution of 5.487 s and 6.585 s, patterns can be deconvolved as well using the shorter acquisitions than using the longer acquisitions employed to develop the methods. As in Figure 4, the red, green, and blue cNMF curves (**left**) from a representative tumor slice (same as in Figure 4) and their corresponding weight maps (**right**) show the spatial distribution and CA uptake behavior of 3 distinct patterns, indicative of well-vascularized (Pattern 1), hypoxic (Pattern 2), and necrotic (Pattern 3) tumor areas, respectively, as previously established (1,2). Decision Maps 1 and 2 were determined as explained in the method section. In Decision Map 1, brown, orange, cyan reflect Pattern1 (indicative of well-vascularized tumor), Pattern 2 (indicative of hypoxia), and Pattern 3 (indicative of necrosis), respectively, while in Decision Map 2, Pattern 3 is displayed as dark blue, Pattern 1 as yellow, Pattern 2 as cyan, and corresponding mixtures as mixture colors.

Shorter acquisition times may affect the overall identifiable shape of the signal-*versus*-time curves, and thus, may affect their criteria for interpretation, e.g. if the acquisition time is so short as to measure no CA washout in well-vascularized areas. Further, tracer-kinetic modeling or semi-quantitative parameters may be affected as well by shortening of acquisition times, depending on model used. Association of patterns with clinically relevant tumor characteristics may also differ from their preclinical interpretation and requiring future research beyond the scope of this study.

Supporting Figure S3

A

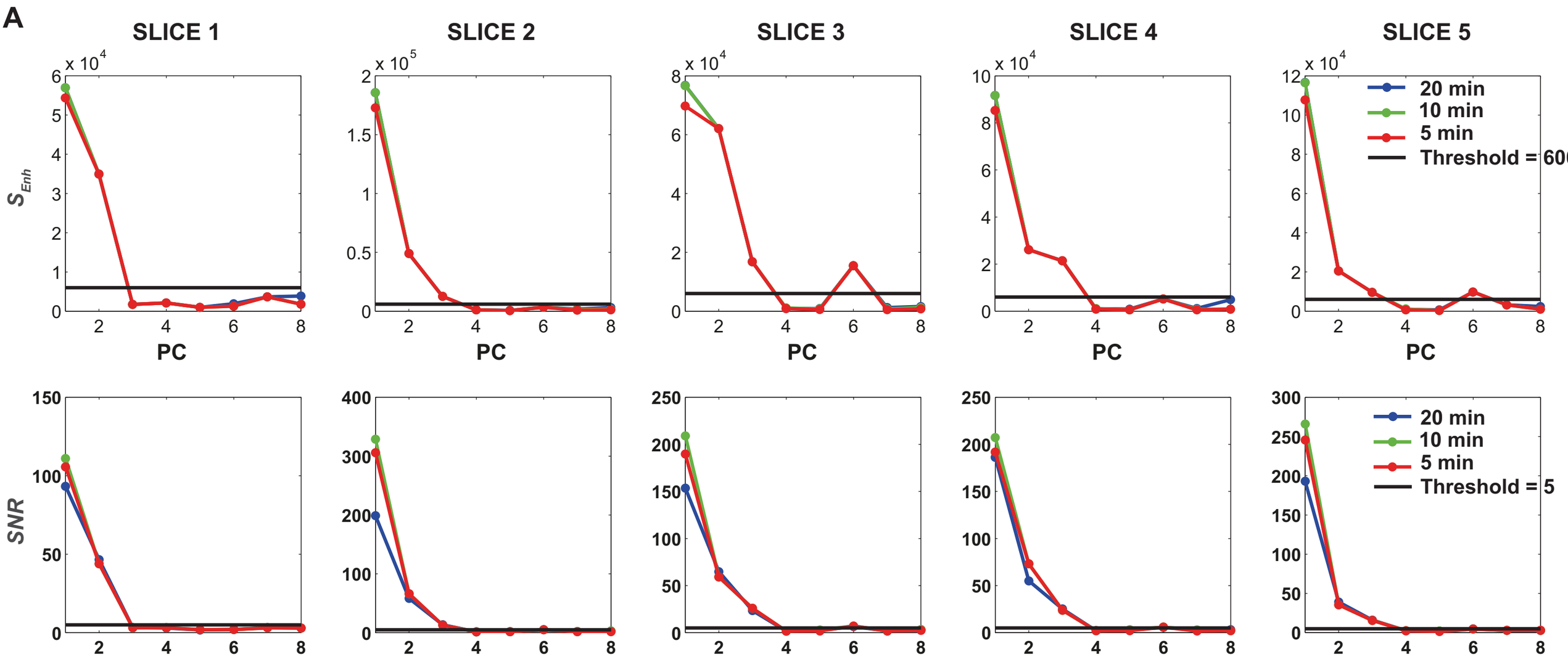

B

Tumor type	#	*HAUC*	SD_{Th}	S_{Enh}	SNR_{Th5}	SNR_{Th2}
HEK	1	1, 4, 4 / 5	1, 1, 1 / 5	5, 5, 5 / 5	5, 5, 5 / 5	5, 5, 5 / 5
	2	2, 3, 0 / 6	2, 1, 1 / 6	6, 6, 6 / 6	6, 6, 6 / 6	6, 6, 6 / 6
	3	0, 5, 2 / 5	1, 0, 0 / 5	4, 4, 4 / 5	5, 5, 5 / 5	5, 5, 5 / 5
	4*	4, 4, 4 / 5	1, 1, 4 / 5	1, 1, 1 / 5	1, 1, 1 / 5	3, 4, 4 / 5
	5	5, 5, 5 / 5	5, 5, 5 / 5	5, 5, 5 / 5	5, 5, 5 / 5	5, 5, 5 / 5
	6	4, 3, 1 / 5	4, 4, 4 / 5	5, 5, 5 / 5	5, 5, 5 / 5	5, 5, 5 / 5
Total		16, 24, 16 / 31	14, 12, 15 /31	26, 26, 26 / 31	27, 27, 27 / 31	29, 30, 30 / 31
		(51.6, 77.4, 51.6%)	(45.2, 38.7, 48.4%)	(83.9, 83.9, 83.9%)	(87.1, 87.1, 87.1%)	(93.5, 96.8, 96.8%)

20 min
10 min
5 min

* Low CNR

C

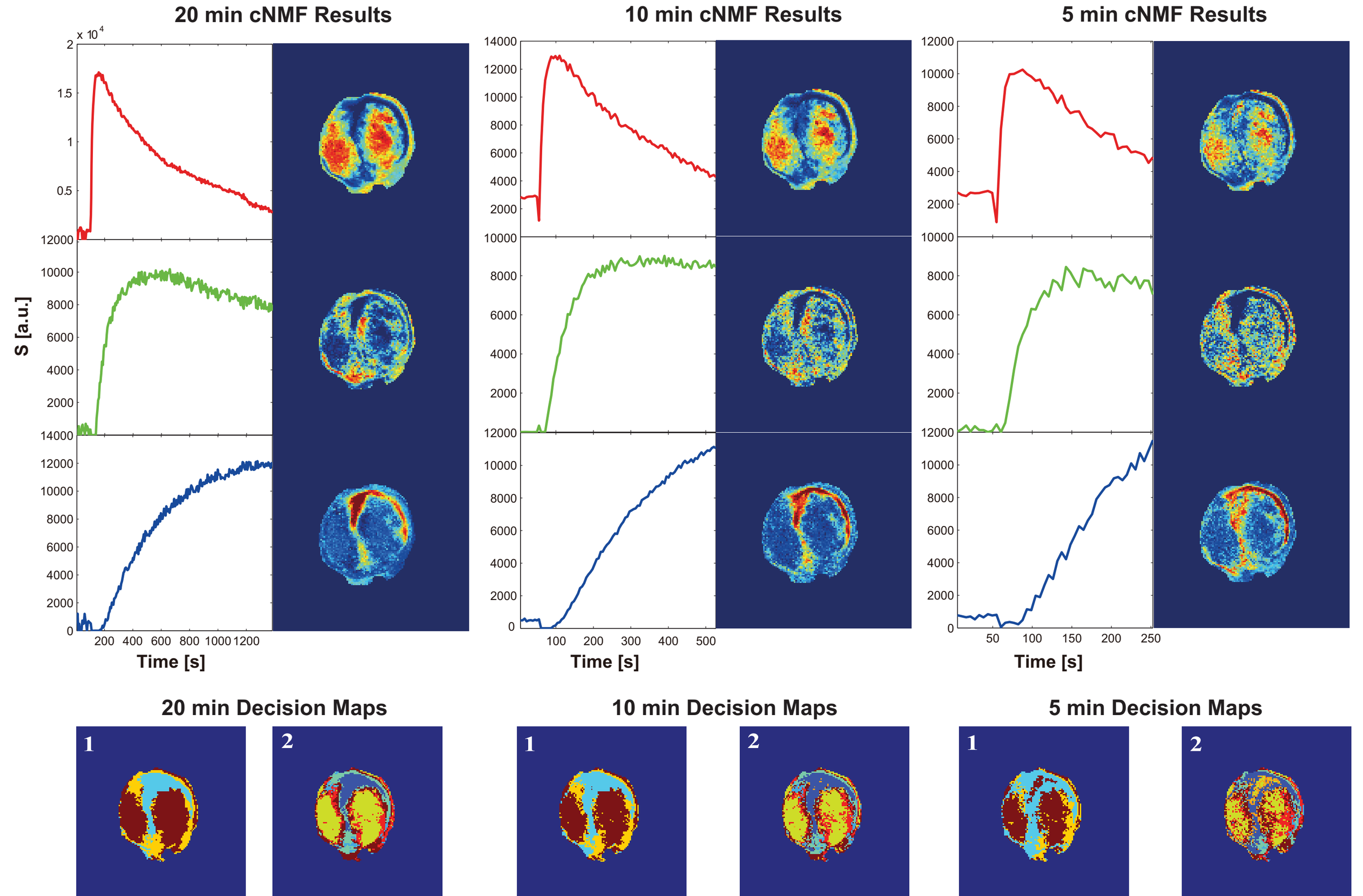

References for Supporting Figures

1. Cho H, Ackerstaff E, Carlin S, Lupu ME, Wang Y, Rizwan A, O'Donoghue J, Ling CC, Humm JL, Zanzonico PB, Koutcher JA. *Noninvasive multimodality imaging of the tumor microenvironment: registered dynamic magnetic resonance imaging and positron emission tomography studies of a preclinical tumor model of tumor hypoxia.* Neoplasia. 2009. Mar; 11(3):247-59, 2p following 259.
2. Stoyanova R, Huang K, Sandler K, Cho H, Carlin S, Zanzonico PB, Koutcher JA, Ackerstaff E. *Mapping Tumor Hypoxia In Vivo Using Pattern Recognition of Dynamic Contrast-enhanced MRI Data.* Transl Oncol. 2012. Dec; 5(6):437-47.